SUPPORTING INFORMATION

Ionic-to-Coordinate Structural Transformation of Hybrid Metal Halides with Improved Anti-Kasha's Room-Temperature Phosphorescence and Dynamic Multicolor Emission

Jie Li[a,b,#], Chenghao Ye[c,#], Siwei Bo[a], Qimin Chen[a], Tianye Su[b], Yingxian Wang[b], Huiting Huang[a], Yunyun Feng[a], Xinyang Chen[a], Xiao-Hong Xiong[b], Qi Pang[a], Binbin Luo[a], and Xianli Li[a,*]

[a] *School of Chemistry and Chemical Engineering and Key Laboratory of Electrochemical Energy Materials, Guangxi University, Nanning 530004, P. R. China*

[b] *Department of Chemistry and Chemical Engineering, Key Laboratory for Preparation and Application of Ordered Structural Materials of Guangdong Province, Shantou University, Shantou 515063, China*

[c] *School of Power and Mechanical Engineering, Wuhan University, Wuhan 430072, P. R. China*

Corresponding Author: lixianli@gxu.edu.cn.

Experimental section

Materials

1H-Pyrazole-4-carbonitrile (98%, Energy), hydrazine dihydrochloride (98%, Sigma-aldrich), indium acetate (99%, Aladdin), antimony(III) chloride (99%, Alfa Aesar), hydrazine hydrate (80%, Xilong Scientific), hydrochloric acid (37%, Guanghua Scientific), ethanol (AR, Guanghua Scientific), ethyl acetate (AR, Guanghua Scientific). All chemicals were used as supplied from commercial sources without further purification.

Synthesis of DPTA

Firstly, solution A was prepared by dissolving 1H-Pyrazole-4-carbonitrile (1.86 g, 20 mmol) in 15 mL of ethanol within a 50 mL beaker under continuous stirring at ambient temperature until complete dissolution (typically 15-20 minutes). Solution B was prepared by combining hydrazine dihydrochloride (2.08 g, 20 mmol) with 3 mL of hydrazine hydrate in a separate 50 mL beaker, followed by sequential stirring (3 minutes) at ambient temperature to obtain a homogeneous clear solution.

After that, solution B was carefully transferred into a 48 mL glass vessel, and solution A was subsequently added. The mixture was subjected to solvothermal reaction at 130 °C for 12 h in an oven. After natural cooling to ambient temperature, colorless needle-like crystals were collected via filtration, washed twice with deionized water and twice with anhydrous ethanol sequentially, and dried under vacuum at 60 °C for 12 h.

Synthesis of In-1 Single Crystal and In-1:x%Sb Single Crystal

DPTA (0.0215 g, 0.1 mmol), indium acetate (0.0292 g, 0.1 mmol), and 2.0 mL of 37 wt% hydrochloric acid were mixed in a 10 mL glass bottle. The mixture was heated under stirring at 120 °C until dissolution, followed by stirring at this temperature for 20 min. After ceasing heating and stirring, the solution was allowed to cool to room temperature, yielding colorless block-shaped crystals. The **In-1** crystals were collected by suction filtration, washed alternately with ethyl acetate and ethanol, and air-dried. For **In-1:x%Sb** samples, DPTA (0.0215 g, 0.1 mmol), indium acetate and antimony chloride (total mole: 0.1 mmol) , and 2.0 mL of 37 wt% hydrochloric acid were mixed in a 10 mL sample vial. The following steps are same with that of **In-1**.

Synthesis of In-2 Single Crystal and In-2:x%Sb Single Crystal

As-synthesized **In-1/In-1:x%Sb** (2.0 g) was loaded into an activation tube and subjected to vacuum activation at 90 °C for 12 h. After cooling to room temperature, the resulting product **In-2/In-2:x%Sb** was obtained.

Synthesis of In-3 Single Crystal and In-3:x%Sb Single Crystal

As-synthesized **In-2/In-2:x%Sb** (2.0 g) was loaded into an activation tube and subjected to vacuum activation at 160 °C for 12 h. After cooling to room temperature, the resulting product **In-3/In-3:x%Sb** was obtained.

Characterization

Single crystal X-ray diffraction (SC-XRD)

SC-XRD tests were conducted on Rigaku XtaLab Pro MM007HF DWX diffractometer at 298 K and 100K using Cu Kα radiation (λ = 1.5418 Å). The structures were solved by intrinsic phasing method using SHELXT[1] program implanted in Olex2[2]. Refinement with full matrix least squares techniques on F2 was performed by using SHELXL[3]. Non-hydrogen atoms were anisotropic ally refined and all hydrogen atoms were generated based on riding mode.

Powder X-ray diffraction (PXRD)

Powder X-ray diffraction (PXRD) measurements for phase identification of samples were performed on a Rigaku MiniFlex600 diffractometer equipped with Cu Kα radiation (λ = 1.5418 Å). Data were collected under ambient conditions at 40 kV and 15 mA, with a 2θ scanning range of 5 - 40°, step size of 0.02°, and scan rate of 10° min^{-1}.

Temperature-dependent PXRD

Thermal stability, phase transition temperatures, and phase evolution of samples were characterized using a Rigaku Ultimalv in-situ high-temperature X-ray diffractometer with Cu Kα radiation (λ = 1.5418 Å). The instrument was operated at 40 kV and 20 mA, with a 2θ scanning range of 5-40°, step size of 0.02°, and scan rate of 10° min^{-1}. The temperature program included a range from 25-250 °C at a heating rate of 10 °C min^{-1} under a nitrogen atmosphere (flow rate: 40.0 mL min^{-1}). Data collection was performed continuously during heating to monitor structural changes dynamically.

Thermogravimetric Analysis (TGA)

Thermal stability, decomposition behavior, and phase transformation characteristics of the samples were evaluated using a TA TGA550 thermogravimetric analyzer. The measurements were conducted under a nitrogen atmosphere at a flow rate of 40 mL min^{-1}, with a temperature range from room temperature to 300 °C and a heating rate of 10 °C min^{-1}. Data were recorded continuously to monitor weight loss and thermal events associated with structural transformations.

Elemental analyses

The elemental analyses of the C and N content is conducted on Elementar (vario EL cube).

Scanning Electron Microscopy (SEM) and Energy Dispersive Spectroscopy (EDS):

Morphological and elemental analyses were performed using a Zeiss Gemini300 field-emission scanning electron microscope equipped with an X-ray energy dispersive spectrometer (EDS). Samples were prepared by ultrasonically dispersing in methanol, drop-casting onto 5 mm × 5 mm silicon wafers, and drying at room temperature for 12 h. The wafers were attached to sample stubs with conductive carbon tape and sputter-coated with gold prior to SEM/EDS measurements. SEM images were acquired at an accelerating voltage of 5–10 kV under high vacuum, while EDS spectra were collected to analyze elemental distributions across the sample surfaces.

Inductively Coupled Plasma Atomic Emission Spectroscopy (ICP-AES)

Quantitative determination of Sb^{3+} content in samples was performed using a Shimadzu ICPE-9000 spectrometer. A calibration curve was constructed with standard solutions containing Sb^{3+} (0–10 ppm), and samples were digested using an optimized acid digestion procedure, followed by appropriate dilution and volume adjustment to meet instrument requirements.

UV-Vis diffusion reflectance spectroscopy

UV-Vis absorption spectra of solid powders were measured using a PerkinElmer LAMBDA 950 spectrometer equipped with an integrating sphere accessory for diffuse reflectance measurements. The spectra were recorded in the wavelength range of 250–800 nm at room temperature, with a scan rate of 200 nm min^{-1} and a slit width of 0.5 nm. A barium sulfate ($BaSO_4$) reference was used for background correction. Data were processed using the Kubelka-Munk transformation to convert reflectance spectra into equivalent absorption coefficients.

Photoluminescence Spectroscopy (PL)

Steady-state emission, excitation luminescence spectra were acquired using a PTI QM-TM system. Samples were placed in quartz slide depressions and positioned in the optical path for measurements. Delayed PL and PL lifetime tests were collected on an Edinburgh FLS 1000 spectrometer. Delayed luminescence decays were analyzed using a time-correlated single-photon counting (TCSPC) module. All data were corrected for instrumental response and background scattering. The PL decay curves are fitted with exponential function as given in the following expression:

$$I(t) = \sum_{n}^{i=1} A_i e^{-\frac{t}{\tau_i}}$$

where $I(t)$ is the PL intensity at time t, A_i represents the relative weights of the decay components, τ_i denotes the decay time for the exponential components. The average lifetime is calculated based on the expression below:

$$\tau_{ave} = \sum_{n}^{i=1} A_i \tau_i^2 \Big/ \sum_{n}^{i=1} A_i \tau_i$$

White-light LED

The doped material was carefully ground and sieved through a 300-mesh screen, then homogenously blended with polydimethylsiloxane (PDMS) at an optimized 3:8 mass ratio. This phosphor-PDMS composite was precisely applied onto a 395 nm UV LED chip and thermally cured at 100 °C for 2 hours to ensure proper adhesion and stability. After cooling to room temperature, the device was encapsulated with a standard LED lens for comprehensive optical characterization.

Computational methodology

We performed first-principles calculations using the Vienna ab initio simulation package (VASP)[4, 5] within the Perdew–Burke–Ernzerhof (PBE) generalized gradient approximation (GGA).[6] A plane-wave basis set with a cutoff energy of 400 eV was employed. The electronic charge density was calculated using a Γ-centered k-grid with dimensions 8 × 8 × 8. Electronic optimizations were performed with a convergence tolerance of 10^{-7} eV, and a Gaussian smearing of 0.04 eV was used to compute the total energy. The projected density of states (PDOS) was obtained to analyze the contributions of individual atomic orbitals to the electronic structure. Van der Waals interactions between the layers were considered using the DFT-D3 method.[7]

Time-dependent density functional theory (TD-DFT) calculations were carried out using the ORCA software package.[8, 9] Three coordination complexes, In-1, In-2 and In-3 were considered in this work. The geometries of the complexes were derived from experimentally determined crystal structures. UV-Vis absorption spectra were simulated at the PBE/DKH-def2-TZVP level of theory using TD-DFT based on the crystal geometries.[10] TD-DFT calculations for three coordination complexes and ε values are showed. For each molecule, the lowest thirty singlet excited states (S1–S30) were computed to capture both π→π* and n→π* transitions relevant to the experimental UV–Vis profile. Oscillator strengths and excitation energies were used to generate stick spectra that were Gaussian-broadened (FWHM = 0.67 eV) to reproduce experimental band envelopes. Agreement of the UV–Vis profile between computational and experimental results confirm the reliability of the computational method. Based on the results of TD-DFT calculation, hole-electron analysis was performed using Multiwfn 3.8 software package.[11]

Table S1. Crystal data of **In-1**, **In-2** and **In-3**.

Sample	**In-1**	**In-2**	**In-3**
Empirical formula	$(C_8H_{11}N_8)InCl_6 \cdot 2.5H_2O$	$(C_8H_{11}N_8)InCl_6$	$(C_8H_7N_8)InCl_4$
Formula weight	591.81	546.77	471.84
Temperature/K	297.99(10)	297.98(10)	100.00(10)
Radiation	Cu *K*α (λ = 1.54184 Å)	Cu *K*α (λ = 1.54184 Å)	Cu Kα (λ = 1.54184 Å)
Crystal system	triclinic	triclinic	triclinic
Space group	$P\bar{1}$	$P\bar{1}$	$P\bar{1}$
a/Å	7.9545(3)	7.5807 (5)	7.096(3)
b/Å	8.1351(3)	7.7002(5)	7.314(3)
c/Å	8.1882(3)	8.0615(5)	8.656(3)
α/°	106.557(3)	76.577(5)	108.03(3)
β/°	105.950(3)	72.818(5)	104.58(3)
γ/°	92.161(3)	87.744(5)	103.97(3)
V/Å^3	484.46(3)	437.08(5)	786.58(6)
Z	1	1	1
ρ_{calc} (g/cm^3)	2.029	2.077	2.021
completeness to θ_{max}	99.3%	97.7%	98.6%
GOF	1.142	1.056	1.066
R_{int}	0.0168	0.1027	0.0754
final *R* indexes [$I > 2\sigma(I)$][a]	R_1 = 0.0205, wR_2 = 0.0553	R_1 = 0.0697, wR_2 = 0.1896	R_1 = 0.1046, wR_2 = 0.2745
R indexes (all data)[a]	R_1 = 0.0206, wR_2 = 0.0553	R_1 = 0.0757, wR_2 = 0.1979	R_1 = 0.1354, wR_2 = 0.3054
largest diff. peak and hole, e Å^{-3}	0.59/-0.58	1.98/-3.21	2.06/-1.92

[a] $R_1 = \Sigma||F_o|-|F_c||/\Sigma|F_o|$; $wR_2 = \{[\Sigma w(F_o^2 - F_c^2)^2]/\Sigma[w(F_o^2)^2]\}^{1/2}$; $w = 1/[\sigma^2(F_o^2)+(aP)^2+bP]$, where $P = [\max(F_o^2, 0) + 2F_c^2]/3$ for all data.

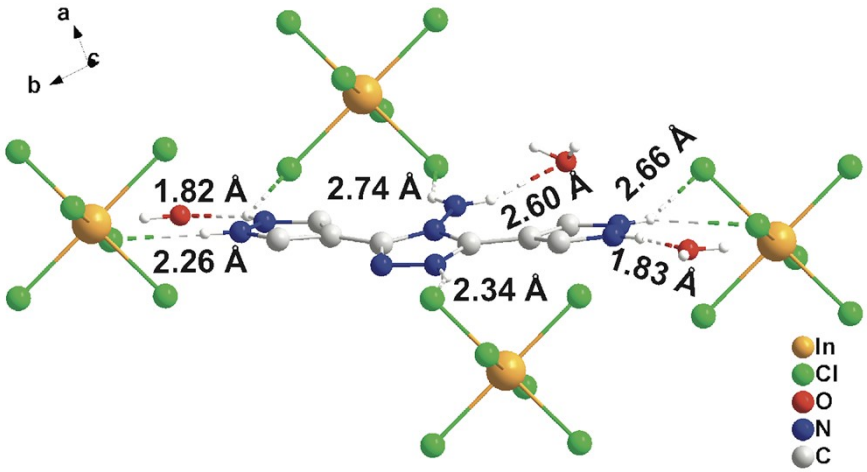

Figure S1. Hydrogen bonding network of **In-1**.

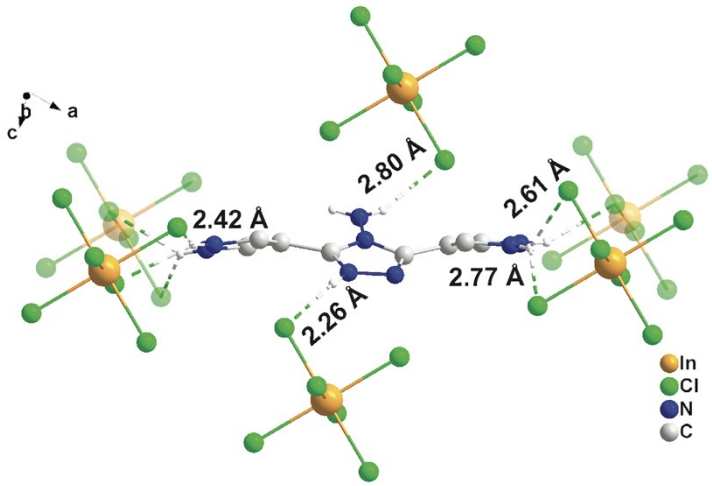

Figure S2. Hydrogen bonding network of **In-2**.

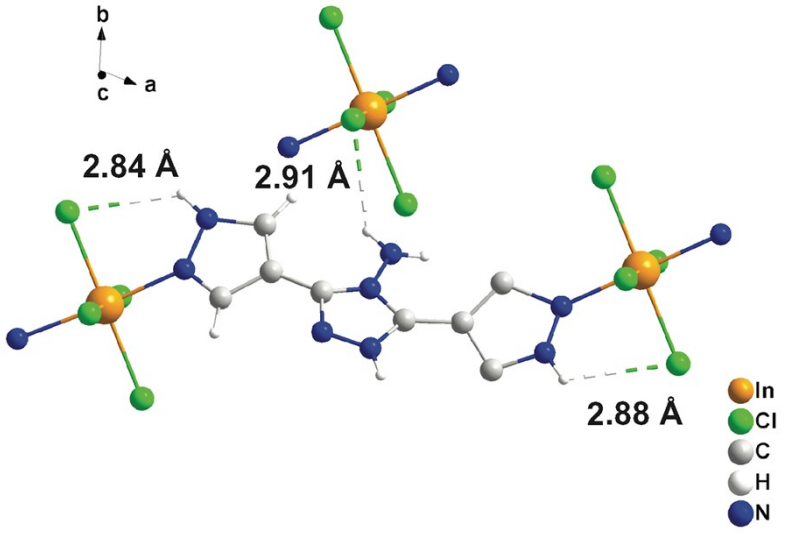

Figure S3. Hydrogen bonding interaction in **In-3**.

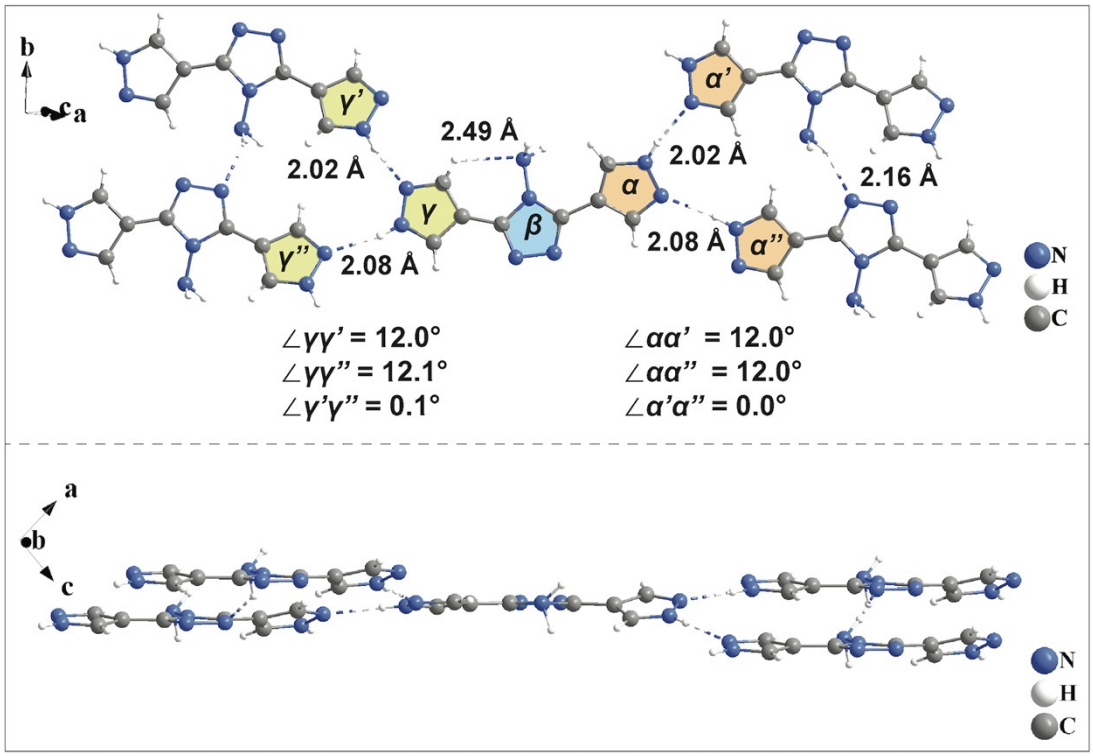

Figure S4. Hydrogen bonding network in DPTA.

Table S2. Elemental analyses data of **In-1**, **In-2** and **In-3**.

wt.%	In-1	In-2	In-3
C	19.03	19.93	24.32
N	18.35	19.21	23.56
at.%	1.21	1.21	1.20

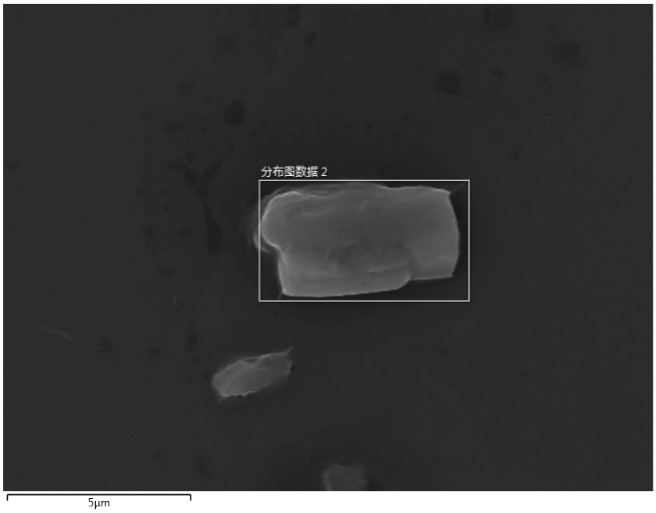

Figure S5. SEM image of **In-1**.

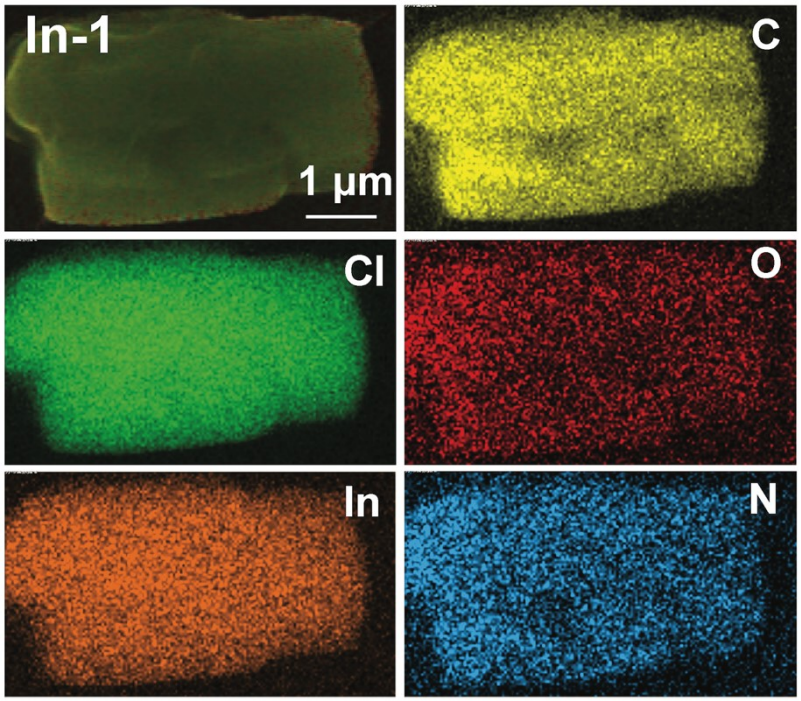

Figure S6. EDS mapping of **In-1**.

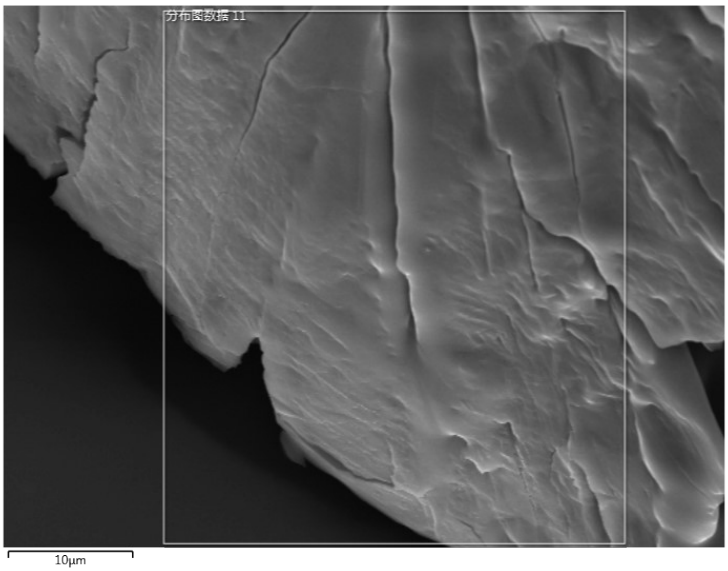

Figure S7. SEM image of **In-2**.

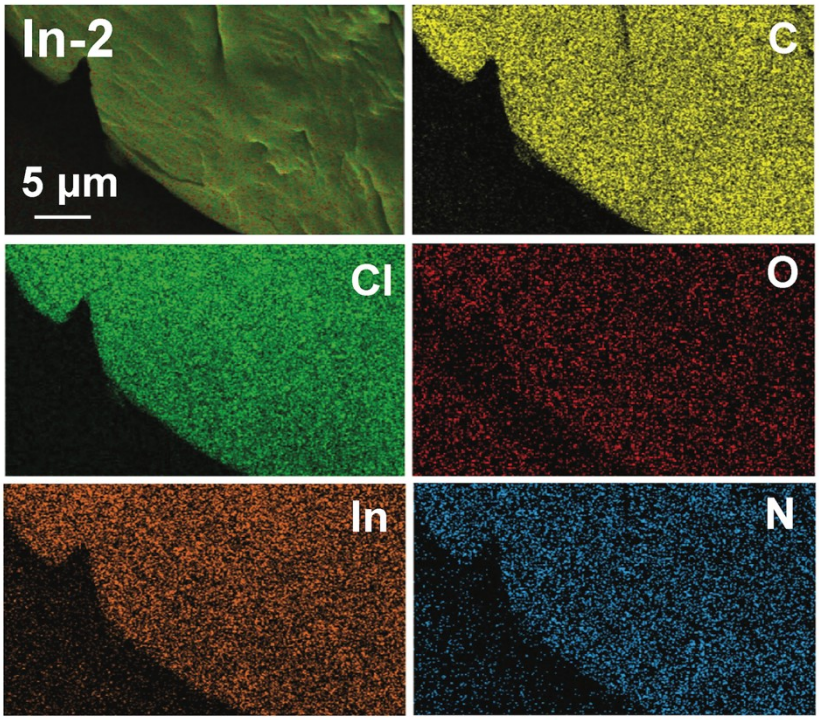

Figure S8. EDS mapping of **In-2**.

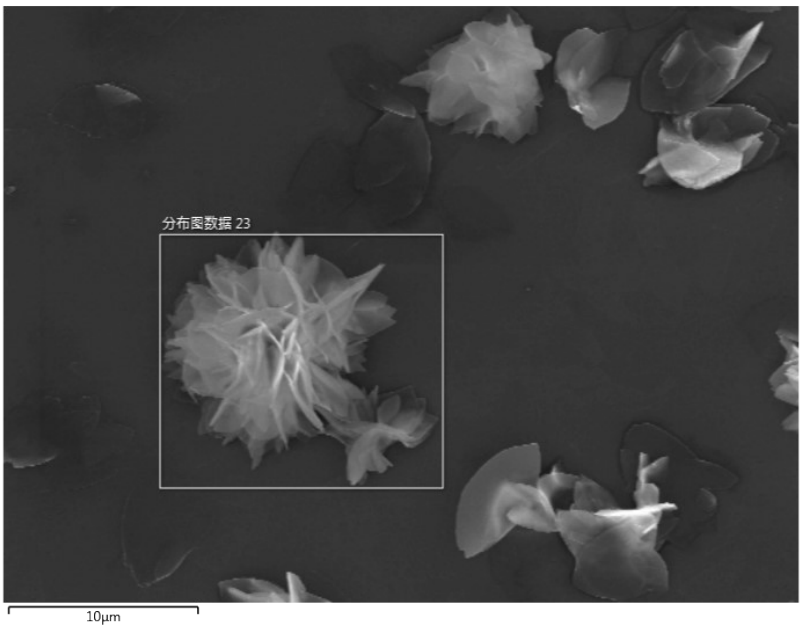

Figure S9. SEM image of **In-3**.

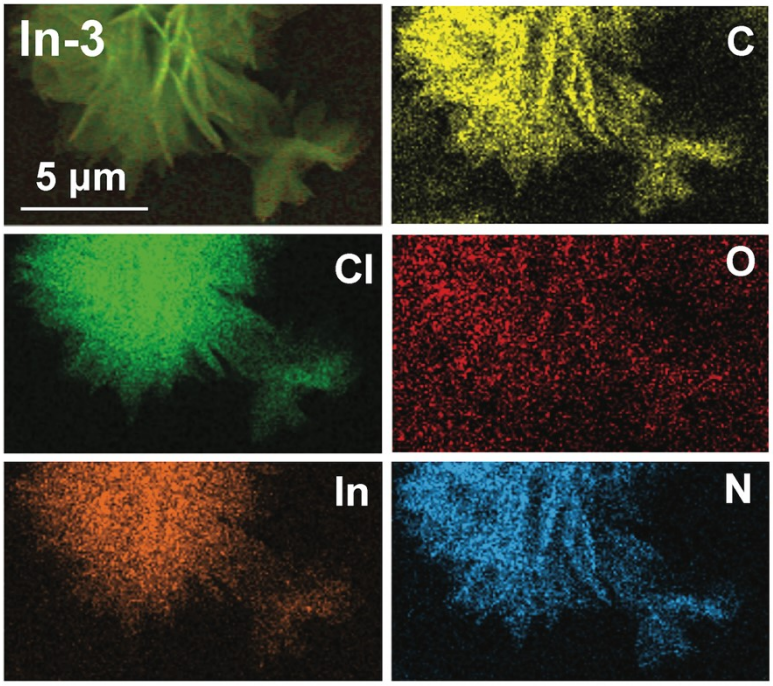

Figure S10. EDS mapping of **In-3**.

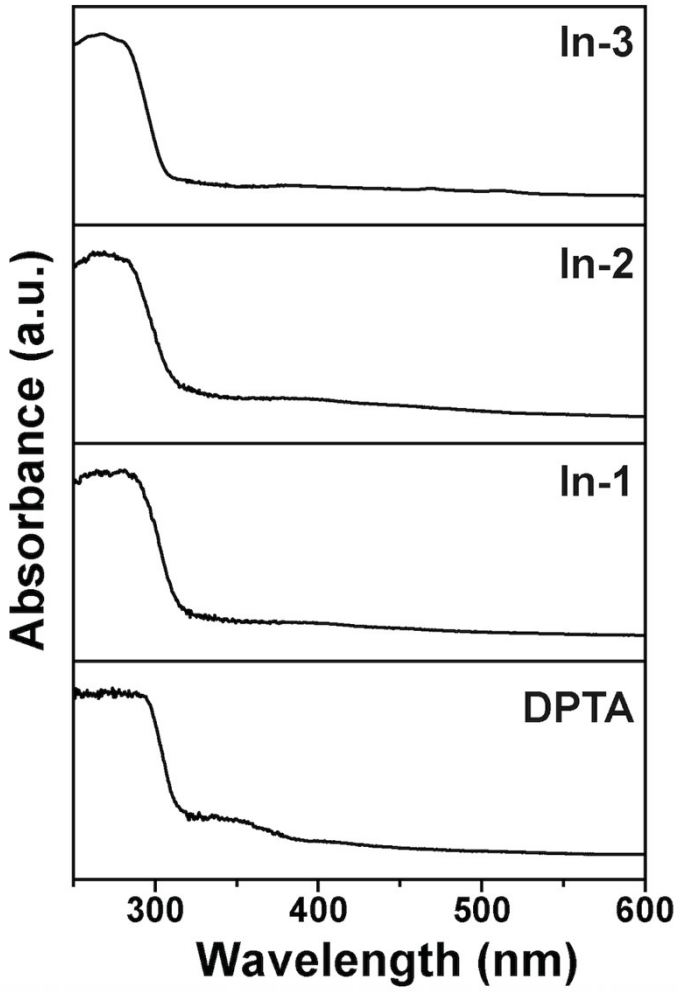

Figure S11. UV-Vis diffusion reflection spectrum of DPTA, **In-1**, **In-2** and **In-3**.

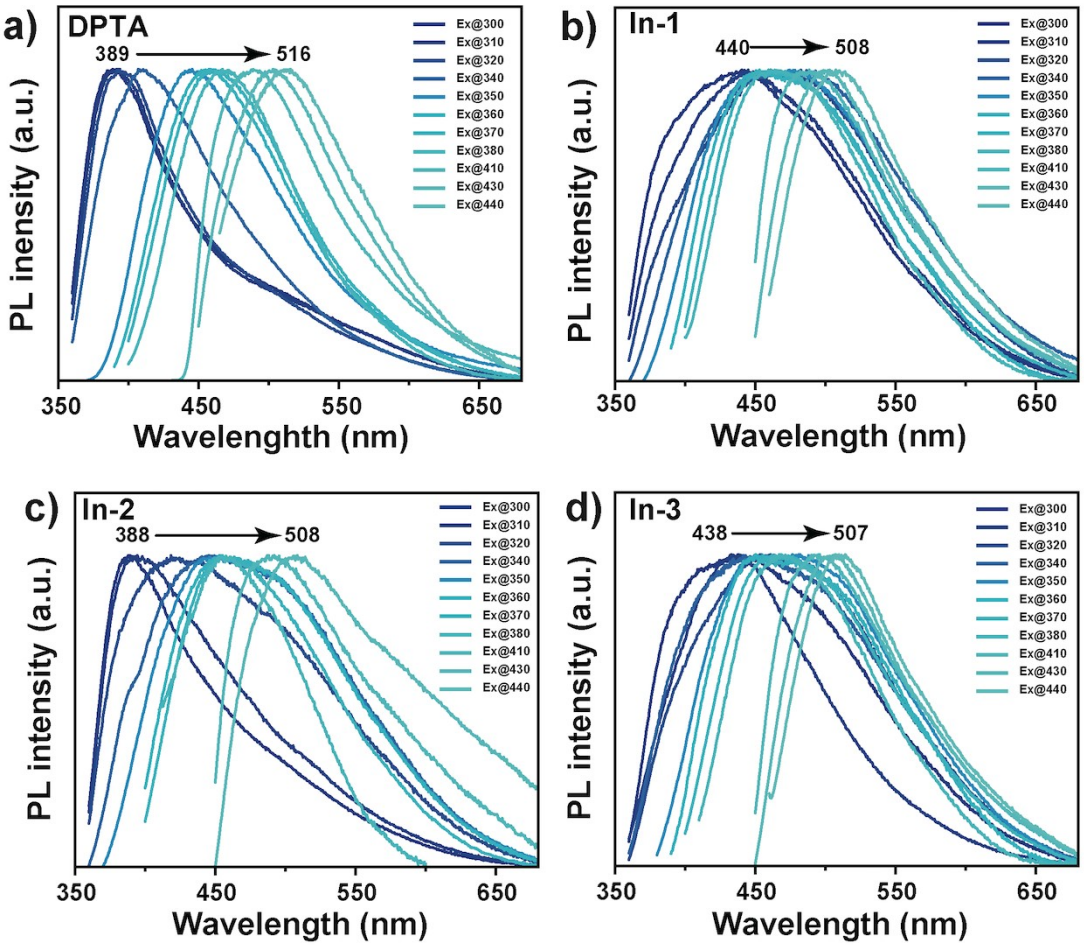

Figure S12. Excitation wavelength-dependent PL spectrum of **In-3**.

Table S3. PLQY of DPTA, **In-1**, **In-2** and **In-3** with different delay time.

Delay time (ms)	DPTA	In-1	In-2	In-3
1	9.1%	8.3%	6.2%	10.9%
10	2.4%	4.2%	8.2%	10.7%
100	1.6%	0.8%	1.0%	2.5%

Table S4. Calculated singlet and triplet energy levels and spin-orbit coupling matrix element (SOCME) values.

Compound	S_1 (eV)	T_n (eV)	ΔE_{ST} (eV)	$\left\|\Psi_{S_1}\right\|\hat{H_{SO}}\left\|\Psi_{T_n}\right\|$
In-1	2.77	2.51 (T_1)	0.26	88.62
		2.64 (T_2)	0.13	113.31
		2.66 (T_3)	0.11	44.24
		2.76 (T_4)	0.01	58.04
		2.78 (T_5)	-0.01	65.77
		2.79 (T_6)	-0.02	28.86
In-2	2.78	2.63 (T_1)	0.15	72.40
		2.67 (T_2)	0.11	79.78
		2.68 (T_3)	0.10	86.11
		2.73 (T_4)	0.05	104.40
		2.79 (T_5)	-0.01	41.49
In-3	2.77	2.49 (T_1)	0.28	134.34
		2.60 (T_2)	0.17	93.74
		2.66 (T_3)	0.11	110.30
		2.72 (T_4)	0.05	26.63
		2.79 (T_5)	-0.02	104.06
		2.80 (T_6)	-0.03	83.90

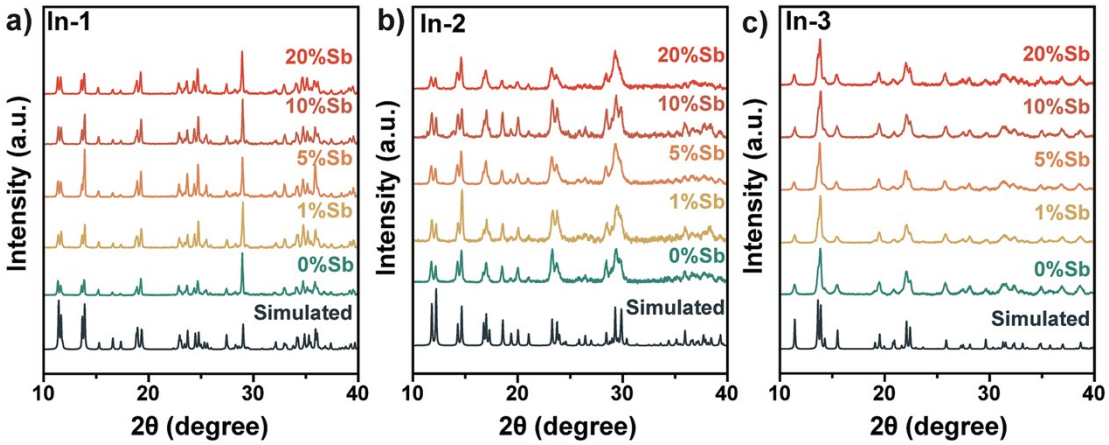

Figure S13. XRD patterns of (a) **In-1:x%Sb**, (b) **In-2:x%Sb** and (c) **In-3:x%Sb**.

Table S5. Sb^{3+} contents of **In-1:x%Sb** detected through ICP-AES.

Samples	Sb atomic ratio
In-1:1%Sb	0.56%
In-1:5%Sb	1.36%
In-1:10%Sb	2.54%
In-1:20%Sb	4.44%

Table S6. Sb^{3+} contents of **In-2:x%Sb** detected through ICP-AES.

Samples	Sb atomic ratio
In-2:1%Sb	0.36%
In-2:5%Sb	1.42%
In-2:10%Sb	2.36%
In-2:20%Sb	4.36%

Table S7. Sb^{3+} contents of **In-3:x%Sb** detected through ICP-AES.

Samples	Sb atomic ratio
In-3:1%Sb	0.16%
In-3:5%Sb	0.76%
In-3:10%Sb	1.89%
In-3:20%Sb	3.40%

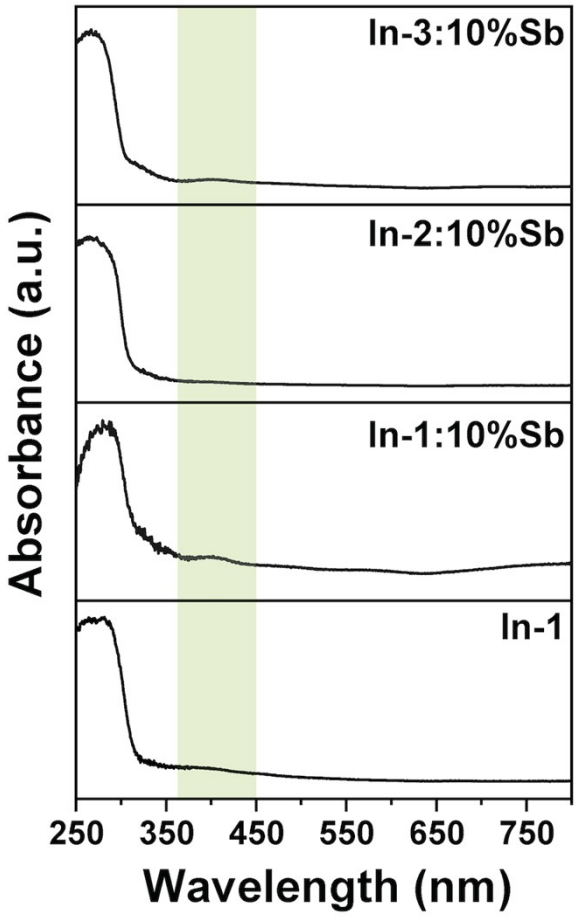

Figure S14. UV-Vis diffusion reflection spectrum of **In-1:10%Sb**, **In-2:10%Sb** and **In-3:10%Sb**.

Table S8. Bond lengths of **In-1**, **In-2**, and **In-3**.

In-1	Bond length/Å	**In-2**	Bond length/Å	**In-3**	Bond length/Å
In-Cl1	2.52	In-Cl1	2.50	In-Cl1	2.47
In-Cl2	2.49	In-Cl2	2.52	In-Cl2	2.47
In-Cl3	2.53	In-Cl3	2.49	In-Cl3	2.47
In-Cl4	2.49	In-Cl4	2.52	In-Cl4	2.47
In-Cl5	2.53	In-Cl5	2.49	In-N1	2.33
In-Cl6	2.52	In-Cl6	2.50	In-N2	2.33

Table S9. Bond angles of **In-1**, **In-2**, and **In-3**.

In-1	Bond angle/°	**In-2**	Bond angle/°	**In-3**	Bond angle/°
Cl1- In-Cl2	90.29	Cl1- In-Cl2	91.73	Cl1- In-Cl2	90.02
Cl1- In-Cl3	89.27	Cl1- In-Cl3	90.12	Cl1- In-Cl3	89.98
Cl1- In-Cl4	89.71	Cl1- In-Cl4	88.27	Cl1- In-N1	87.25
Cl1- In-Cl5	90.73	Cl1- In-Cl5	89.88	Cl1- In-N2	89.46
Cl2- In-Cl3	90.14	Cl2- In-Cl3	90.15	Cl2- In-N1	89.26
Cl3- In-Cl4	89.86	Cl3- In-Cl4	89.85	N1-In-Cl3	90.74
Cl4- In-Cl5	90.14	Cl4- In-Cl5	90.15	Cl3-In-N2	89.65
Cl2- In-Cl5	89.86	Cl2- In-Cl5	89.85	Cl2- In-N2	90.35
Cl6- In-Cl2	89.71	Cl6- In-Cl2	88.27	Cl4- In-Cl2	89.98
Cl6- In-Cl3	90.73	Cl6- In-Cl3	89.88	Cl4- In-Cl3	90.02
Cl6- In-Cl4	90.29	Cl6- In-Cl4	91.73	Cl4- In-N1	92.75
Cl6- In-Cl5	89.27	Cl6- In-Cl5	90.12	Cl4- In-N2	90.54

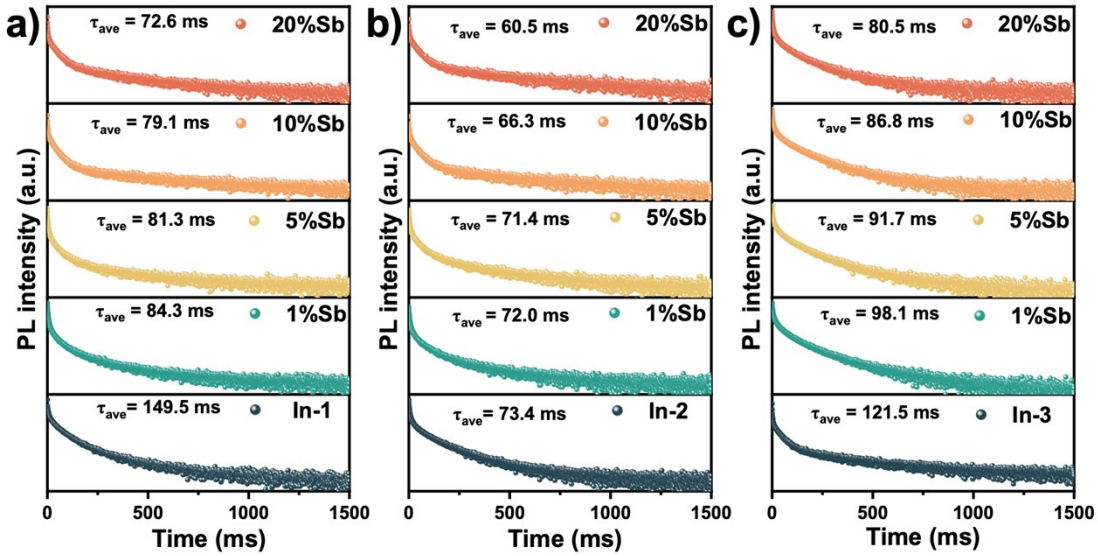

Figure S15. PL decay curves of **In-1:10%Sb**, **In-2:10%Sb** and **In-3:10%Sb** at 520 nm.

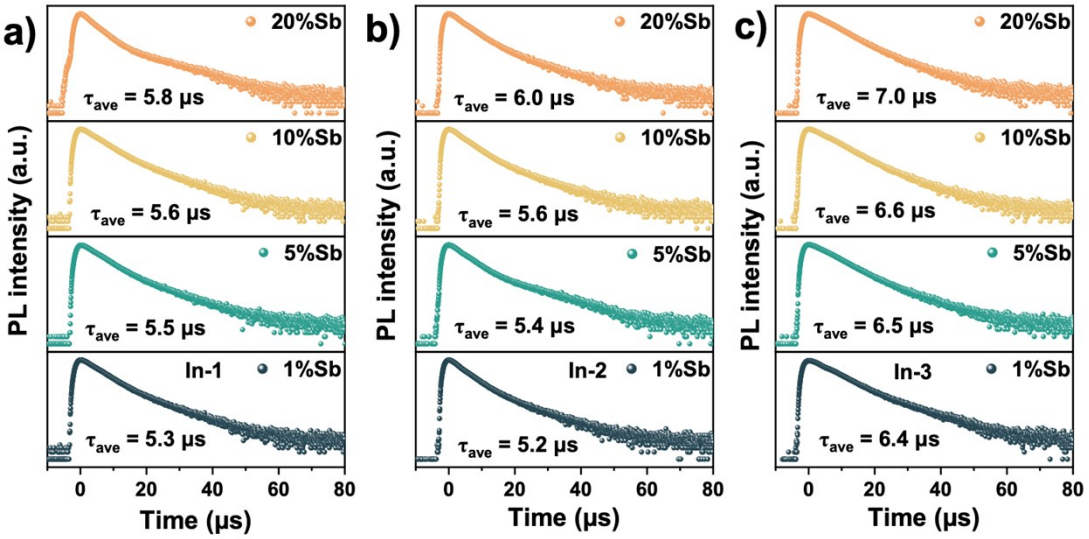

Figure S16. PL decay curves of **In-1:10%Sb** at 580 nm, **In-2:10%Sb** at 550 nm and **In-3:10%Sb** at 650 nm.

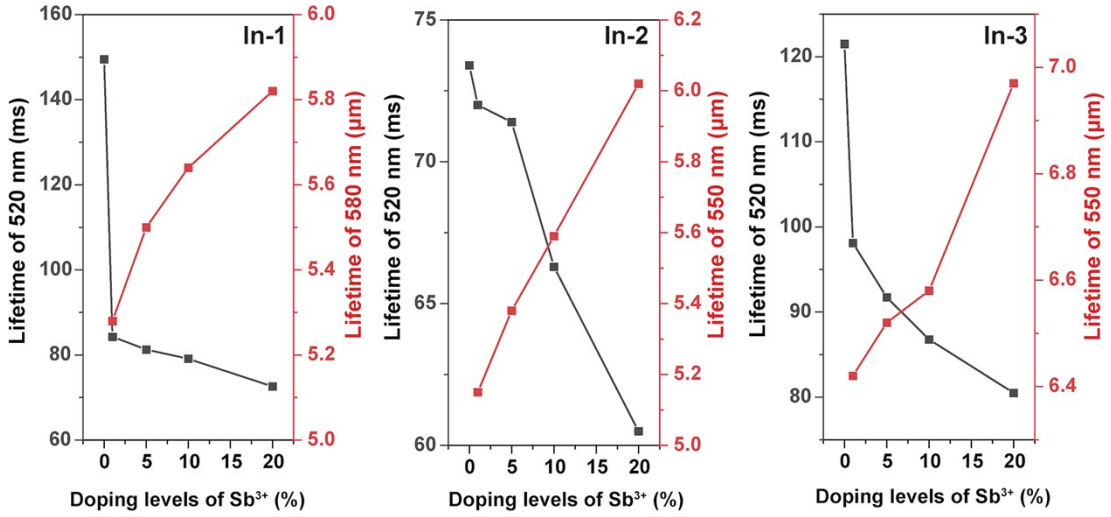

Figure S17. Evolution of PL lifetime of **In-1**, **In-2** and **In-3**

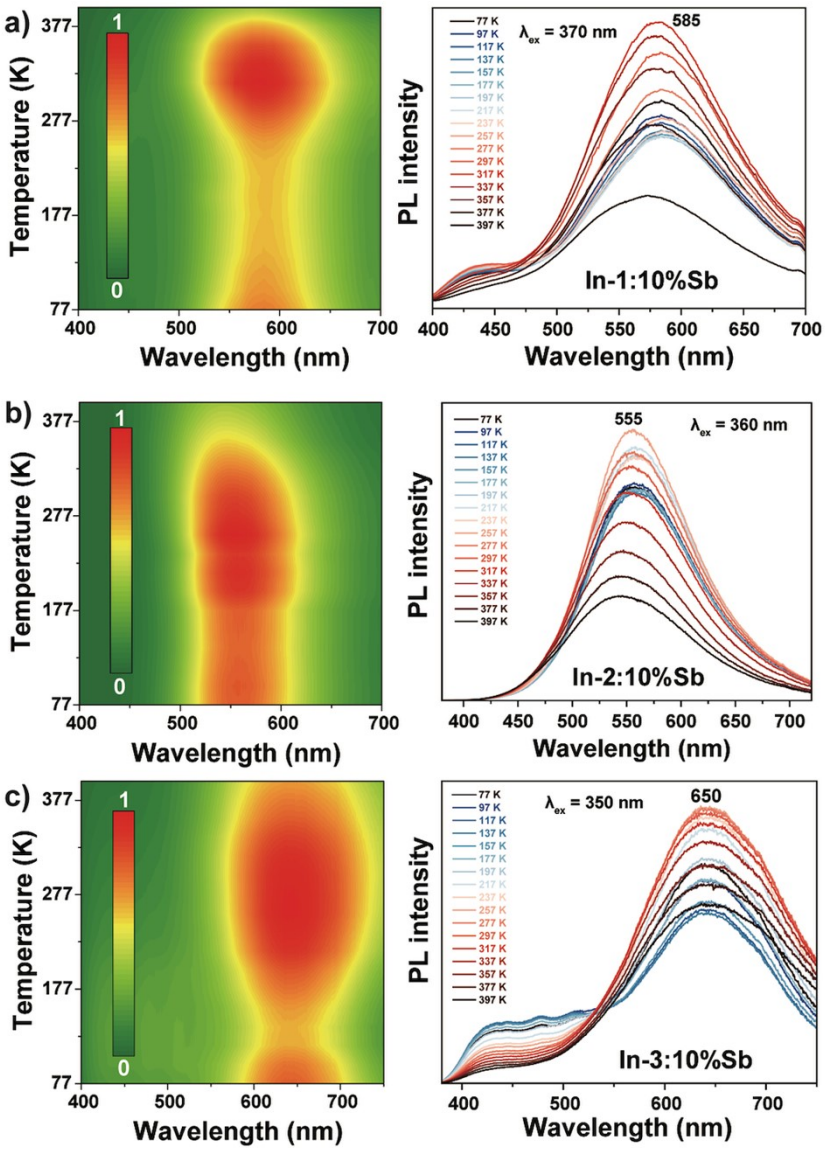

Figure S18. Temperature-dependent PL of (a) **In-1:10%Sb**, (b) **In-2:10%Sb** and (c) **In-3:10%Sb**.

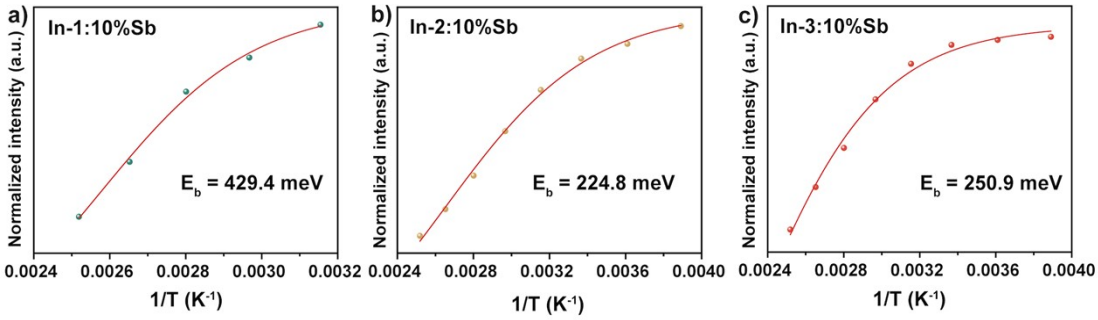

Figure S19. Plot of PL intensity as a function of temperature to calculate E_b of (a) **In-1:10%Sb**, (b) **In-2:10%Sb** and (c) **In-3:10%Sb**.

The Cartesian Coordinates of the complexes.

In-1

Cl	-0.99376300	0.22711700	1.81923500
Cl	-4.65098400	-0.14105700	1.44243700
Cl	-2.71185600	1.39910900	-1.14299900
O	-2.35124000	4.55265500	-0.56573400
H	-2.74144300	5.45293900	-0.52839100
H	-3.03931100	3.96547000	-0.94125900
H	-0.21728700	1.82458600	-0.95149800
H	-0.90472500	4.20632300	-0.40463300
H	0.97823100	5.41578400	0.63349200
H	3.09475000	3.97871500	0.91671500
H	5.11938400	1.85207500	1.34016100
N	0.08624200	3.77431800	-0.23932800
N	1.11353700	4.44310900	0.32206300
C	2.55129800	1.15897700	-0.12559700
C	0.47473500	2.52589900	-0.49337600
C	2.17760600	3.64102200	0.45050500
C	1.81120800	2.38729000	-0.06873900
H	5.55212100	1.97526100	-0.27708000
N	3.88455000	0.95569500	0.07243500
N	4.76776200	1.98950100	0.38175900
H	1.07143300	-0.32538300	-0.63465500
N	2.98061300	-1.01959500	-0.37821200
N	2.04667000	-0.04913400	-0.39043400
H	7.05120600	0.11700200	0.86657600

H	8.45085600	-2.08279300	0.46829300
H	7.15921900	-3.77470700	-0.51364500
H	4.72459700	-3.09394400	-0.98499500
N	7.42736000	-1.86263300	0.25567500
N	6.70645200	-2.85260400	-0.30607800
C	4.11686300	-0.40237500	-0.09834800
C	6.64785600	-0.78654100	0.42205400
C	5.45814400	-2.44403500	-0.52019500
C	5.36577700	-1.12046800	-0.05416200
In	-2.65350600	-0.82733600	0.10285400
Cl	-4.07326000	-1.90806100	-1.70693700
Cl	-0.59585400	-1.42991500	-1.36813400
Cl	-2.39666800	-3.01791900	1.27398300

In-2

Cl	0.64640900	-2.22787900	-0.82860500
Cl	2.40384200	-1.72070900	2.26508800
Cl	0.07446000	0.67372400	1.22321200
N	-1.60261400	5.07561400	-0.04462500
N	-0.61626300	4.43162000	-0.70437800
N	-3.46757500	1.39965200	1.26558000
H	-1.50068700	6.08324300	0.21931700
H	0.29770300	4.89010800	-0.94913200
H	-0.21072100	2.44099900	-1.26534800
H	-3.43651900	4.53081800	0.84096500
H	-3.60584000	2.04465400	2.07794600
H	-1.03135200	0.00130000	-1.53434400

C	-0.90632200	3.13267500	-0.79443900
C	-2.14389200	2.93358300	-0.15312400
C	-2.55076800	4.20039100	0.30708000
C	-2.75589500	1.67139100	0.16825800
In	2.06738400	-0.39636300	0.10896900
Cl	4.08358500	-1.48232600	-1.06713200
Cl	1.64332700	1.01200600	-2.02084600
Cl	3.59713900	1.43186400	0.97661200
N	-3.82392300	0.10172800	1.34830300
N	-3.19632600	-3.94791400	-0.68907800
N	-4.35077500	-3.89795100	0.00505100
H	-2.47941400	-0.29001400	-2.32528800
H	-2.79966800	-4.82434000	-1.09990100
H	-4.86844100	-4.76933500	0.25770900
H	-5.44133700	-2.38645300	1.01254500
H	-1.69557300	-2.57221200	-1.23662100
C	-3.32089700	-0.45873700	0.26281800
C	-4.56720800	-2.64398100	0.42069600
C	-3.49840400	-1.85738200	-0.04496800
C	-2.65193500	-2.72996000	-0.74697200
N	-2.64788900	0.48883800	-0.49592900
N	-1.97849200	0.36434600	-1.70992600

In-3

C	1.54744500	1.04379600	0.00000000
C	1.85823100	3.25470300	-0.03231800
C	2.35788100	2.07313200	0.52191100

C	3.41562800	1.77091800	1.44904400
H	1.62549800	-0.02677800	0.15009400
H	2.15498100	4.29661100	0.06945300
H	0.17962800	3.52600300	-1.31324500
N	0.62261900	1.55633600	-0.80780400
N	0.82835800	2.89487400	-0.82349700
H	4.99512800	3.40895800	-0.02004400
H	4.60736100	4.38807500	1.28061600
N	4.61900700	2.43625400	1.65181100
N	5.13014900	3.55333300	0.98944000
N	3.38009500	0.67129800	2.18397700
Cl	8.43405900	3.31993900	7.65548400
C	7.19477600	3.18123900	3.56015000
C	7.44046500	0.95986300	3.69159900
C	6.60779000	1.95691100	3.16378300
C	5.33208300	1.70273100	2.55408500
H	9.23707600	1.17057600	4.81031200
H	6.84818700	4.19650400	3.40757000
H	7.38721500	-0.12320800	3.64762700
H	4.80480500	-0.18047400	3.40182100
N	8.29915400	2.93421500	4.27364000
N	8.42397200	1.59054400	4.34076300
N	4.55123800	0.66198700	2.84774700
Cl	7.99229700	6.08797900	5.52404300
In	9.63636100	4.22370200	5.67110000
Cl	11.28043300	2.35943300	5.81815400
Cl	10.83866200	5.12745500	3.68671000

Cl	11.06870100	5.60493700	7.16799400
H	-0.08422000	1.05297100	-1.30479600

References

1. Sheldrick, G., SHELXT - Integrated space-group and crystal-structure determination. *Acta Crystallographica Section A* **2015**, 71 (1), 3-8.

2. Dolomanov, O. V.; Bourhis, L. J.; Gildea, R. J.; Howard, J. A. K.; Puschmann, H., OLEX2: a complete structure solution, refinement and analysis program. *J. Appl. Crystallogr.* **2009**, 42 (2), 339-341.

3. Sheldrick, G., A short history of SHELX. *Acta Crystallographica Section A* **2008**, 64 (1), 112-122.

4. Kresse, G.; Hafner, J., Ab initio molecular-dynamics simulation of the liquid-metal–amorphous-semiconductor transition in germanium. *Physical Review B* **1994,** *49* (20), 14251.

5. Kresse, G.; Furthmüller, J., Efficiency of ab-initio total energy calculations for metals and semiconductors using a plane-wave basis set. *Computational Materials Science* **1996,** *6* (1), 15-50.

6. Kresse, G.; Furthmüller, J., Efficient iterative schemes for ab initio total-energy calculations using a plane-wave basis set. *Physical review B* **1996,** *54* (16), 11169.

7. Grimme, S.; Antony, J.; Ehrlich, S.; Krieg, H., A consistent and accurate ab initio parametrization of density functional dispersion correction (DFT-D) for the 94 elements H-Pu. *The Journal of Chemical Physics* **2010,** *132* (15).

8. Neese, F., The ORCA program system. *Wiley Interdisciplinary Reviews: Computational Molecular Science* **2012,** *2* (1), 73-78.

9. Neese, F., Software update: the ORCA program system—version 6.0. *Wiley Interdisciplinary Reviews: Computational Molecular Science* **2025,** *15* (2), e70019.

10. Laurent, A. D.; Jacquemin, D., TD-DFT benchmarks: a review. *Int. J. Quantum Chem* **2013,** *113* (17), 2019-2039.

11. Lu, T.; Chen, F., Multiwfn: A multifunctional wavefunction analyzer. *Journal of Computational Chemistry* **2012,** *33* (5), 580-592.